

A mathematical approach to computing structural-failure boundaries

H.M. Osinga

Department of Mathematics, University of Auckland, New Zealand

ABSTRACT: Earthquakes can cause substantial damage to buildings in ways that are still not well understood. The magnitude and principal frequency of an earthquake are two primary components that affect the extent of the damage, and they are the basis for many design specification guidelines. We investigate how an external force with varying magnitude and principal frequency affects structural stability. As an example we consider a model of a planar, post-tensioned frame that exhibits dynamics quite similar to the experimental measurements of a scaled model on a shake table. Our goal is to predict behaviour of models subject to an aperiodic external force (an earthquake). Here, we consider a periodic external force, which is a simplifying but common choice. Many results in the literature are obtained from performing a large number of simulations over a range of magnitudes and frequencies. Our approach is much more efficient and uses a novel computational method that approximates the failure boundary directly. We find that failure can occur in profoundly different ways, due to inherent nonlinearities in the system. Stability is particularly affected if the natural frequency of the structure is close to that of the external forcing.

1 INTRODUCTION

There have been quite a number of earthquakes recently, including in New Zealand, that raised the awareness of a need for earthquake resistant buildings. Most notorious is the 2011 Christchurch earthquake, which followed a series of earthquakes starting in September 2010 and provides a striking example of the need for better damage assessment (Kam et al. 2011). First and foremost, we like to have buildings that do not collapse during an earthquake so that lives are saved; even better, the building should be such that it sustains virtually no damage from any earthquake below a critical magnitude, so that costly reparations can be avoided and it can safely be used again after the event. Ideas for low-damage design include allowing a degree of damage at predefined locations that do not affect the safety of inhabitants (Priestley et al. 1999, Qin et al. 2013), and activating rigid body movement of structural members so that forces related to local deformation in the structure will be prevented (Acikgoz & De Jong 2012, Alexander et al. 2011, Fardis & Rakicevic 2012). Furthermore, mathematical models are developed that complement the experimental results with detailed numerical analysis (Alexander et al. 2011, Oddbjornsson et al. 2012).

A major drawback of the theoretical research is the fact that the earthquake is typically modelled by a sine wave, which effectively means that the theoretical results underestimate the resilience of the model. The main argument against using more complicated external forcing terms is the simplicity of reducing the system to an autonomous equation. The response of such systems is governed by periodic solutions that have the same period as the sinusoidal earthquake, which implies that the analysis can be done with standard software packages. We explore a different approach that offers the possibility of computing failure boundaries of the model directly, without the need to formulate the system in autonomous form. As an example, we consider the model of a tied rocking block on an elastic foundation, which is equivalent to that of a planar, post-tensioned frame on a shake table (Alexander et al. 2011). For such frames, the joints between beam-columns and column-foundations are held together by pre-stressed cables, and the elastic nonlinearity of the frame is entirely determined by mechanics of these joint connections. The system dynamics

can then be described in terms of a standardised (non-dimensional) angle φ that is equal to ± 1 at the point of joint opening. This leads to the equation

$$\begin{cases} \ddot{\varphi} + 2\gamma\dot{\varphi} + \mu(\varphi) = A \sin(\omega t), \\ |\varphi(t)| < \varphi_{\max} \quad \text{for all } 0 \leq t \leq T_{\text{end}}, \end{cases} \quad (1)$$

where, the dot represents derivation with respect to time t . The maximum angle φ_{\max} depends on the characteristics of the building and T_{end} is some maximum integration time that represents the duration of the earthquake. The stiffness function $\mu(\varphi)$ is given by

$$\mu(\varphi) = \begin{cases} \varphi, & |\varphi| \leq 1, \\ \left(\frac{3}{\beta} + \frac{12}{\beta^2} + \frac{8}{\beta^3} \right) \varphi \\ + \left(3 + \frac{9}{\beta} + 6\frac{1-\sqrt{\psi}}{\beta^2} - 6\frac{\sqrt{\psi}}{\beta^3} - 2\frac{\psi\sqrt{\psi}}{\beta^3\varphi^2} \right) \text{sgn}(\varphi), & |\varphi| > 1, \end{cases}$$

where $\psi = (1 + \beta)(\varphi^2 + \beta|\varphi|)$ and β is the contact-to-cable stiffness ratio; see (Alexander et al. 2011) for details. Solutions φ to (1) are called *admissible* if $|\varphi(t)| < \varphi_{\max}$ for all t . We use the same parameters as in (Alexander et al. 2011), that is, we fix $\beta = 85$, $\gamma = 0.05$ and $\varphi_{\max} = 10$, and we consider periodic ground motion with varying frequency ω and amplitude A . Here, ω and A are non-dimensional parameters; the frequency ω is the ratio between the actual forcing frequency and the natural frequency of the frame; and the amplitude A is given by the peak ground acceleration relative to the scaled angle and the storey height of the building.

We are particularly interested in the solution $\varphi(t)$ of (1) that satisfies the initial condition $(\varphi(0), \dot{\varphi}(0)) = (0, 0)$; we denote this solution by $\Phi_0(t)$. Our goal is to understand how admissibility of $\Phi_0(t)$ depends on the forcing frequency ω and amplitude A . Since the forcing is periodic, any bounded solutions will eventually be periodic. Consequently, it seems reasonable to expect that it is possible to predict admissibility of $\Phi_0(t)$ from the admissibility of the limiting periodic orbit. We argue that such prediction is not possible, not even in an approximating sense.

2 FORCING WITH FIXED FREQUENCY $\omega = 0.575$

For a range of pairs (ω, A) in the frequency-amplitude plane, there exist three different periodic orbits and two of these are stable. Such bistability is well known to occur in nonlinear oscillator systems like system (1). Let us consider $\omega = 0.575$ fixed and consider the A -dependent family of periodic orbits, which can readily be computed, for example, via pseudo-arclength continuation with the software package AUTO (Doedel 2007).

2.1 Admissibility of periodic orbits

If the forcing amplitude $A = 0$ then the periodic orbit has zero amplitude and is, in fact, equal to $\Phi_0(t)$. Starting from this solution, we can compute a one-parameter family of periodic orbits by increasing A . Figure 1(a) shows the result of such a continuation with respect to A , where $\omega = 0.575$ is kept fixed at a value that is representative for a large range of forcing frequencies; here, we plot the maximum angle of the periodic orbit versus A . For small A , only one periodic orbit exists, which has low amplitude and is stable; we denote it by \mathcal{A}_ℓ . We checked that $|\Phi_0(t)| < \varphi_{\max}$ for all t when the forcing is chosen from the regime in the (ω, A) -plane for which only \mathcal{A}_ℓ exists; hence, \mathcal{A}_ℓ is always admissible. Provided A is small enough, $\Phi_0(t)$ accumulates onto \mathcal{A}_ℓ .

As A increases, a fold bifurcation gives rise to a pair of periodic orbits, an attractor \mathcal{A}_h and a saddle \mathcal{S}_m , that have much larger amplitudes than \mathcal{A}_ℓ . For $\omega = 0.575$, this fold bifurcation occurs at $A \approx 0.4897$. The fold bifurcation marks the beginning of a bistable regime during which the amplitude of the attractor \mathcal{A}_ℓ increases and that of the saddle \mathcal{S}_m decreases until \mathcal{A}_ℓ and \mathcal{S}_m merge and disappear at a second fold bifurcation; for $\omega = 0.575$, the second fold bifurcation occurs at $A \approx 1.1282$. For large A , only the attractor \mathcal{A}_h exists and $\Phi_0(t)$ accumulates onto \mathcal{A}_h . As indicated in Figure 1(a), the maximum of φ along \mathcal{A}_h exceeds φ_{\max} from $A \approx 0.7151$. Indeed, also for other forcing frequencies, the high-amplitude attracting periodic orbit \mathcal{A}_h is not admissible for large values of A . Therefore, $\Phi_0(t)$ is not admissible for large A either.

Figure 1(b) shows the co-existence of three periodic orbits for the parameter pair $(\omega, A) = (0.575, 0.6)$ in projection onto the $(\varphi, \dot{\varphi})$ -plane. Observe that \mathcal{A}_ℓ has low amplitude and is clearly

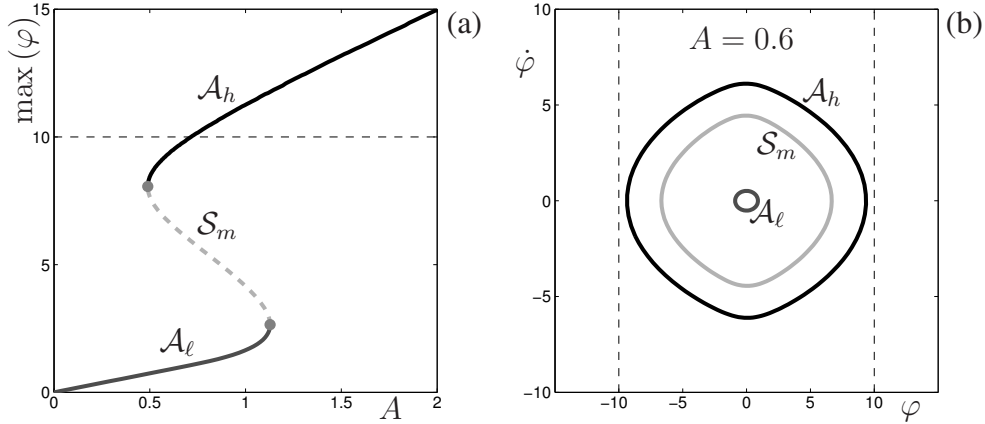


Figure 1. Periodic orbits of system (1) in dependence on the forcing amplitude A , where $\omega = 0.575$ is fixed. Panel (a) shows A on the horizontal axis and the amplitude of the periodic orbit on the vertical axis. Panel (b) shows three co-existing periodic orbits for $A = 0.6$ in the bistable regime plotted in projection onto the $(\varphi, \dot{\varphi})$ -plane. The low- and high-amplitude periodic orbits labelled \mathcal{A}_l and \mathcal{A}_h , respectively, are stable, while the mid-amplitude periodic orbit labelled \mathcal{S}_m is of saddle type.

admissible, while the amplitude for \mathcal{A}_h is so high that it is almost equal to φ_{\max} . Note that the maximum angle of these periodic orbits is exactly the same as their minimum angle, because of the symmetry $(\varphi, \dot{\varphi}, t) \mapsto (-\varphi, -\dot{\varphi}, t + \pi/\omega)$ of system (1). For $(\omega, A) = (0.575, 0.6)$, the solution $\Phi_0(t)$ is admissible and it accumulates onto \mathcal{A}_l .

2.2 Unexpected failure

Let us now consider the parameter pair $(\omega, A) = (0.575, 1.0607)$ for which there are still three co-existing periodic orbits, \mathcal{A}_l , \mathcal{S}_m and \mathcal{A}_h . For this higher value of A , the periodic orbits \mathcal{A}_l and \mathcal{A}_h are both stable, but \mathcal{A}_h is no longer admissible. Figure 2 shows the time series of $\Phi_0(t)$ overlayed on \mathcal{A}_l in panel (a) and on \mathcal{S}_m in panel (b), with the corresponding projections onto the $(\varphi, \dot{\varphi})$ -plane, in panels (c) and (d), respectively; included in panel (d) is the periodic orbit \mathcal{A}_h , which is not admissible. Observe from panel (a) that $\Phi_0(t)$ eventually accumulates onto \mathcal{A}_l , while panel (b) illustrates how $\Phi_0(t)$ first appears to accumulate onto \mathcal{S}_m . Panels (c) and (d) clearly show that $|\Phi_0(t)|$ is much smaller than φ_{\max} for all t .

Even though Figure 2 provides no indication of imminent danger, the amplitude $A = 1.0607$ is very close to the failure boundary for $\omega = 0.575$. Indeed, $\Phi_0(t)$ is not admissible when the amplitude is only slightly larger. Figure 3 shows the behaviour of $\Phi_0(t)$ for the parameter pair $(\omega, A) = (0.575, 1.0610)$. The figure is similar to Figure 2, showing the time series of $\Phi_0(t)$ in panels (a) and (b) and the corresponding phase portraits in the $(\varphi, \dot{\varphi})$ -plane in panels (c) and (d), respectively. As in Figure 2, the solution $\Phi_0(t)$ again appears to accumulate onto \mathcal{S}_m initially, but then, instead of decreasing in amplitude towards \mathcal{A}_l , the amplitude of $\Phi_0(t)$ increases and $\Phi_0(t)$ accumulates onto \mathcal{A}_h . Since \mathcal{A}_h is not admissible, admissibility of $\Phi_0(t)$ is also lost at this A -value. We note that failure of $\Phi_0(t)$ only occurs after a relatively long time in the admissible regime, which means that serious damage is only sustained if the duration of the forcing at this frequency and amplitude is long enough.

Observe that the maximum amplitude of $\Phi_0(t)$ is, in fact, larger than the amplitude of \mathcal{A}_h . Hence, for this value of ω , the transition from accumulation onto \mathcal{A}_l to accumulation onto \mathcal{A}_h occurs well after \mathcal{A}_h loses admissibility, but it appears that loss of admissibility of \mathcal{A}_h is not a necessary condition for $\Phi_0(t)$ to fail. We also note that the point of failure of $\Phi_0(t)$ for this forcing frequency occurs well before the fold bifurcation at $A \approx 1.1282$, where \mathcal{A}_l and \mathcal{S}_m disappear. We estimate the precise A -value for $\omega = 0.575$ at which $\Phi_0(t)$ fails to be $A \approx 1.0608$. At this value, $\Phi_0(t)$ accumulates onto \mathcal{S}_m instead of \mathcal{A}_l or \mathcal{A}_h . Such behaviour is special, because \mathcal{S}_m is not attracting. It means that $\Phi_0(t)$ is contained in the stable manifold of \mathcal{S}_m , which is a surface in $(\varphi, \dot{\varphi}, t)$ -space that separates the basins of attraction of \mathcal{A}_l and \mathcal{A}_h . As illustrated in Figures 2 and 3, just before and just after loss of admissibility, respectively, neither the admissibility of the periodic orbits, nor the extent of the bistability regime can serve as a good approximation of the

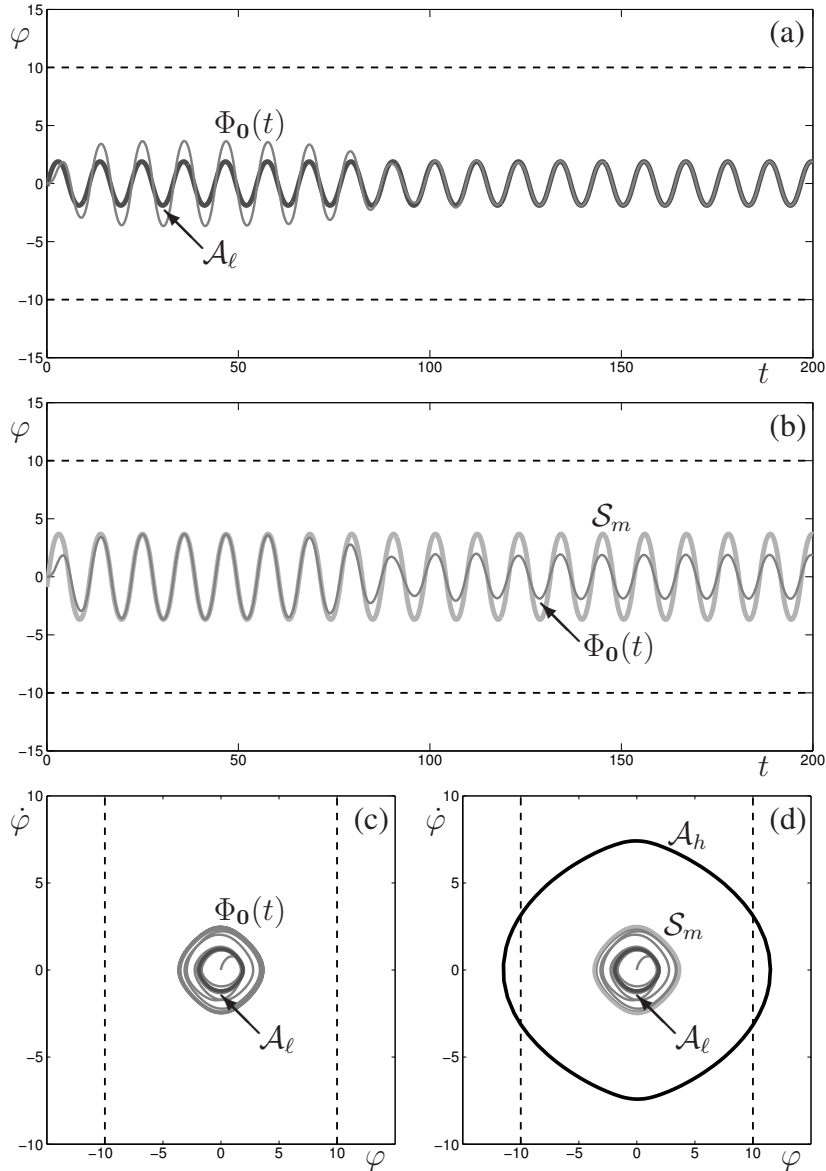


Figure 2. The solution $\Phi_0(t)$ of system (1) with $(\omega, A) = (0.575, 1.0607)$. Panel (a) compares the time series of $\Phi_0(t)$ with that of \mathcal{A}_ℓ and panel (b) with that of \mathcal{S}_m . The corresponding projections in the $(\varphi, \dot{\varphi})$ -plane are shown in panels (c) and (d), respectively.

failure boundary. This means that the simplifying assumption of a periodic earthquake does not offer any benefit from an analytical point of view to help predict this type of failure.

3 FORCING WITH FIXED FREQUENCY $\omega = 0.675$

While the hard-to-predict failure described in the previous section occurs over a range of forcing frequencies, not all forcing frequencies lead to failure of this type. There also exists a range of values for ω at which $\Phi_0(t)$ fails in a more predictable manner, namely, at which its amplitude increases in direct proportion with A until $|\Phi_0(t)| = \varphi_{\max}$ for some $0 < t \leq T_{\text{end}}$. However, this type of failure can also not be predicted by studying the behaviour of the periodic orbits.

As an example, we consider $\omega = 0.675$, for which $\Phi_0(t)$ fails at $A \approx 0.9535$. At these values of ω and A , only one periodic orbit exists, \mathcal{A}_h , which is admissible. Figure 4 shows the time series of $\Phi_0(t)$ at this (ω, A) -pair, overlaid on the time series of \mathcal{A}_h . Even though \mathcal{A}_h is admissible, the solution $\Phi_0(t)$ converges to it in a non-monotonic way and the angle φ of $\Phi_0(t)$ exceeds the amplitude of \mathcal{A}_h during the transient approach to it. As shown in Figure 4, at about $t = 28.86$,

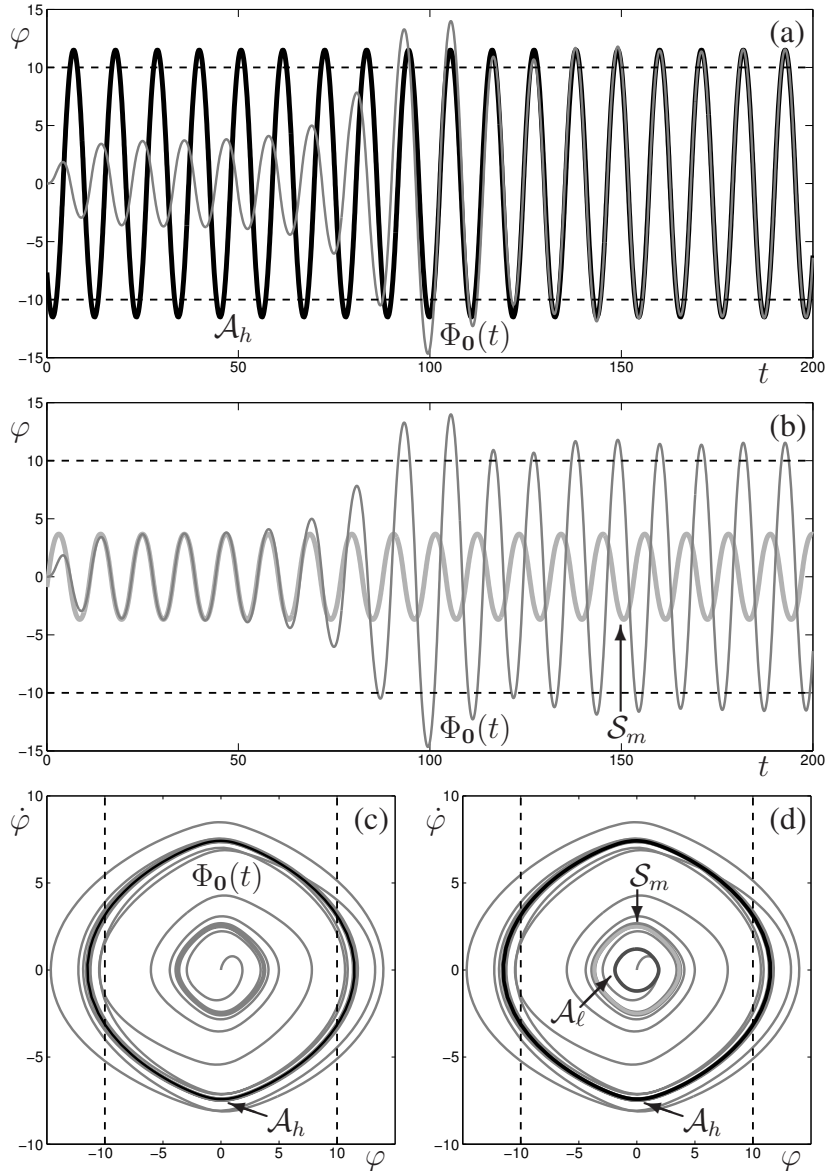


Figure 3. The solution $\Phi_0(t)$ of system (1) with $(\omega, A) = (0.575, 1.0610)$. Panel (a) compares the time series of $\Phi_0(t)$ with that of \mathcal{A}_h and panel (b) with that of \mathcal{S}_m . The corresponding projections in the $(\varphi, \dot{\varphi})$ -plane are shown in panels (c) and (d), respectively.

the angle φ of $\Phi_0(t)$ grazes the boundary $\varphi = -10$, before $\Phi_0(t)$ converges to \mathcal{A}_h . For slightly smaller A , the minimum of φ along $\Phi_0(t)$ remains just above $\varphi = -10$, while for slightly larger A , it will lie just below this lower bound.

While this type of failure is more gradual, it is important to realise that the periodic orbit \mathcal{A}_h gives no indication of imminent failure, nor does the fact that there is no bistability for this value of A . The high-amplitude periodic orbit \mathcal{A}_h only reaches the maximum amplitude of 10 when $A \approx 1.8043$ for $\omega = 0.675$. Furthermore, the low-amplitude periodic orbit \mathcal{A}_ℓ for $\omega = 0.675$ exists up until $A \approx 0.8278$, at which it merges with the saddle periodic orbit \mathcal{S}_m that appears in a fold bifurcation at $A \approx 0.3771$. Hence, also for this type of failure, there is no benefit, from an analytical point of view, in assuming that the earthquake is periodic.

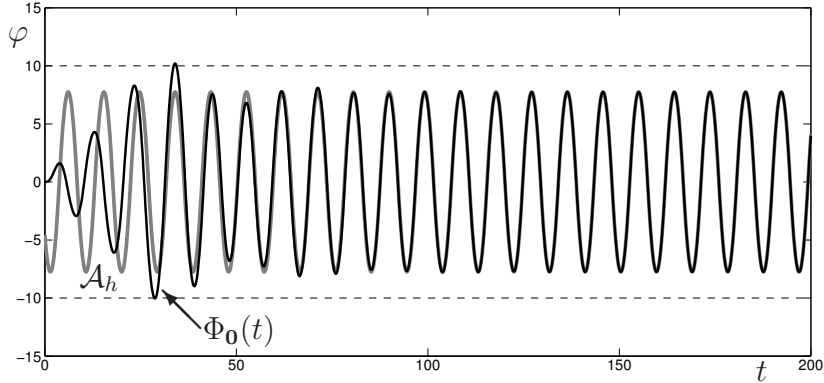


Figure 4. Time series of $\Phi_0(t)$ for $\omega = 0.675$ and $A = 0.95354140$, approximately at the moment of failure. The only existing periodic orbit at these parameter values, which is the high-amplitude periodic orbit \mathcal{A}_h , is also shown.

4 FAILURE BOUNDARY IN THE (ω, A) -PLANE

We now consider admissibility of $\Phi_0(t)$ in dependence on both ω and A . Our approach is to approximate the moment of failure as the family of solutions $\Phi_0(t)$ that are tangent to the boundary of the admissible regime $\varphi(t) \in [-10, 10]$ for some $0 < t < T_{\text{end}}$; such a solution is called a *grazing solution*. Grazing solutions can be computed accurately, as is explained in the next section.

There are two types of grazing solutions: either $\Phi_0(t)$ is first tangent to the boundary $\varphi = -10$, which we call a left-grazing event, or $\Phi_0(t)$ is first tangent to the boundary $\varphi = +10$, which we call a right-grazing event. For any given frequency ω , there is typically more than one amplitude A for which $\Phi_0(t)$ is a grazing solution, and the failure boundary is defined as the curve with minimal amplitudes $A = A(\omega)$ for which there are grazing events. Figure 5 shows all curves of left- and right-grazing events for $\Phi_0(t)$ in the range $(\omega, A) \in [0.1, 1] \times [0.8, 2.6]$, up to total integration time $T_{\text{end}} = 150$; the darker-shaded curves, labelled g_L , correspond to left-grazing events and the lighter-shaded curves, labelled g_R , are right-grazing events. The choice $T_{\text{end}} = 150$ corresponds to about 10 periods of the forcing for $\omega = 0.575$, but substantially fewer or more periods when ω is close to 0.1 or 1, respectively.

There are no grazing events for $A < 0.8$. For larger A -values, a main resonance tongue can be discerned that approximately ranges over values $\omega \in [0.3, 1]$. This main resonance tongue is composed of curves along which $\Phi_0(t)$ alternately grazes the left and right admissibility boundary. Note that the failure boundary is piecewise smooth, with a discontinuity in its slope at each point where a curve g_L meets a curve g_R . At such a double grazing event, $\Phi_0(t)$ is a left-grazing solution that also exhibits a right-grazing event at some later time $t < T_{\text{end}}$, or $\Phi_0(t)$ is a right-grazing solution that also exhibits a left-grazing event at some later time $t < T_{\text{end}}$. Hence, the failure boundary is not only piecewise smooth, there is also a discontinuity in the time at which grazing occurs when there is a double-grazing event. For example, if $\omega = 0.675$, the solution $\Phi_0(t)$ is admissible for all A below the first grazing event at $A \approx 0.9535$, at which $\Phi_0(t)$ exhibits a left-grazing event for $t \approx 28.86$. As ω increases, $\Phi_0(t)$ continues to graze the boundary $\varphi = -10$, where the time of grazing varies continuously with ω until $\omega \approx 0.6956$. For this value of ω , the solution $\Phi_0(t)$ grazes the boundary $\varphi = -10$ when $t \approx 28.64$, but also the boundary $\varphi = +10$ for $t \approx 23.55$, which is about half a period earlier. Hence, for slightly larger values of ω , the solution $\Phi_0(t)$ fails in a right-grazing event at a time approximately half a period earlier than before.

Note the accumulation of left- and right-grazing events for a range of values ω , including $\omega = 0.575$. Here, the failure boundary is characterised by the fact that $\Phi_0(t)$ accumulates on \mathcal{S}_m instead of one of the two attractors \mathcal{A}_ℓ or \mathcal{A}_h , as described in Section 2.2.

Figure 5 also shows what could be interpreted as second and perhaps third harmonics that have not been fully resolved. Here, the value $T_{\text{end}} = 150$ represents only up to five periods of the forcing. It seems that other grazing events at higher periods form part of the failure boundary for

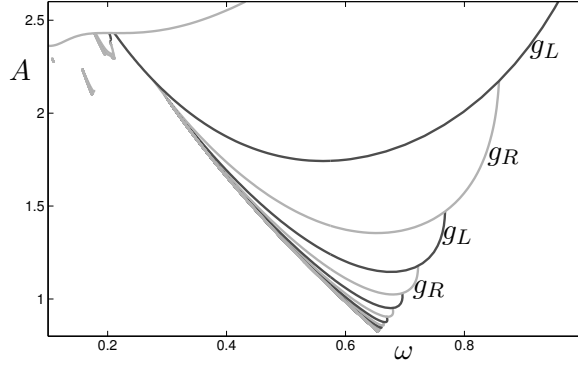


Figure 5. Left-grazing (g_L) and right-grazing (g_R) events for the solution $\Phi_0(t)$ of system (1) with $(\varphi, \dot{\varphi}) = (0, 0)$ at $t = 0$.

these smaller ω -values, but a detailed investigation of this low-frequency regime is left for future work.

5 DIRECT COMPUTATIONAL METHOD

We now present an algorithm that computes the failure boundary directly as a curve in the (ω, A) -plane. Grazing events can be computed numerically by continuation of a two-point boundary value problem. To this end, we rewrite (1) as a system of first-order differential equations

$$\dot{\mathbf{u}} = T \mathbf{f}(\mathbf{u}), \quad (2)$$

where $\mathbf{u} = \{\mathbf{u}(s) := (\varphi(sT), \dot{\varphi}(sT), sT) \mid 0 \leq s \leq 1\}$ represents a trajectory or orbit segment of a solution φ of (1) up to time T . The orbit segment \mathbf{u} is formulated in scaled time such that it is always defined on the interval $[0, 1]$. We impose boundary conditions to ensure that the orbit segment starts with the particular initial condition $(\varphi, \dot{\varphi}) = (0, 0)$ at time $t = 0$, and ends at a grazing point:

$$\begin{cases} \mathbf{u}(0) &= (0, 0, 0), \\ \mathbf{u}(1) &= (\pm 10, 0, 1). \end{cases} \quad (3)$$

With the integration time T and the frequency-amplitude pair (ω, A) as free parameters, system (2)–(3) is well posed and gives rise to one-parameter solution families that correspond to the left- and right-grazing events.

We use pseudo-arclength continuation with the software package AUTO (Doedel 2007) to find the left- and right-grazing solution families. To start the continuation, we first compute $\Phi_0(t)$ as the solution of system (1) starting from $\varphi = 0$ and $\dot{\varphi} = 0$ with $\omega = 0.575$ and $A = 5.0$; the high value of A ensures that $\Phi_0(t)$ crosses the admissibility boundaries $\varphi = \pm 10$ many times. We then use AUTO to find the values A below 5.0 at which $\Phi_0(t)$ exhibits a grazing event for $\omega = 0.575$ fixed, even when the event occurs after $\Phi_0(t)$ failed. Each of those grazing events can then be continued in ω and A to form a branch in the left- or right-grazing solution family.

ACKNOWLEDGEMENTS

I am grateful to Chris Budd for helpful discussions on the geometry of the failure boundary. This research is supported by grant # 3712132 from the Engineering Faculty Research Development Fund of The University of Auckland.

REFERENCES

Acikgoz, S. & De Jong, M.J. 2012. The interaction of elasticity and rocking in flexible structures allowed to uplift. *Earthquake Engineering and Structural Dynamics* **41**(15): 2177–2194.

- Alexander, N.A., Oddbjornsson, O., Taylor, C.A., Osinga, H.M. & Kelly, D.E. 2011. Exploring the dynamics of a class of post-tensioned, moment resisting frames. *Journal of Sound and Vibration* **330**(15): 3710–3728.
- Doedel, E.J. 2007. AUTO-07P: Continuation and bifurcation software for ordinary differential equations. With major contributions from Champneys, A.R., Fairgrieve, T.F., Kuznetsov, Yu.A., Oldeman, B.E., Paffenroth, R.C., Sandstede, B., Wang, X.J. & Zhang, C.; available at <http://cmvl.cs.concordia.ca/auto>.
- Fardis, M.N. & Rakicevic, Z.T. 2012. *Role of Seismic Testing Facilities in Performance-Based Earthquake Engineering: SERIES Workshop*. Heidelberg: Springer-Verlag.
- Kam, W.Y., Pampanin, S. & Elwood, K. 2011. Seismic performance of reinforced concrete buildings in the 22 February Christchurch (Lyttelton) earthquake. *Bulletin of the New Zealand Society for Earthquake Engineering* **44**(4): 239–278.
- Oddbjornsson, O., Alexander, N.A., Taylor, C.A., & Sigbjörnsson, R. 2012. Numerical and experimental exploration of the fundamental nonlinear dynamics of self-centring damage resistant structures under seismic excitation. in: 15th World Conference of Earthquake Engineering, Lisbon, # 4670, 10 pages.
- Osinga, H.M. 2014. Computing failure boundaries by continuation of a two-point boundary value problem. in: Cunha, A., Caetano, E., Ribeiro, P., Muller, G. (Eds.) Proceedings of the 9th International Conference on Structural Dynamics, EURO-DYN 2014, Porto #MS10-263, pp. 1891–1897.
- Priestley, M.J.N., Sriharan, S., Conley, J.R. & Pampanin, S. 1999. Preliminary results and conclusions from the PRESSS five-story precast concrete test building. *PCI Journal* **44**(6): 42–67.
- Qin, X., Chen, Y. and Chouw, N. 2013. Effect of uplift and soil nonlinearity on plastic hinge development and induced vibrations in structures. *Advances in Structural Engineering* **16**(10): 135–147.